

pubs.acs.org/cm Article

Unified Understanding of Molecular Weight Dependence of Electron Transport in Naphthalene Diimide-Based n-Type Semiconducting Polymers

Duyen K. Tran, Amélie Robitaille, I Jo Hai, Chia-Chun Lin, Daiki Kuzuhara, Tomoyuki Koganezawa, Yu-Cheng Chiu, Mario Leclerc, and Samson A. Jenekhe*



Cite This: Chem. Mater. 2022, 34, 9644-9655



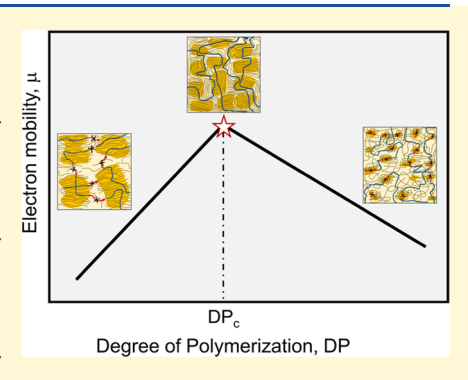
ACCESS I

III Metrics & More

Article Recommendations

Supporting Information

ABSTRACT: Electron transport is critical to the use of n-type semiconducting polymers in diverse electronic and optoelectronic devices. Herein, we combine measurements of field-effect electron mobility and bulk electron mobility with thin-film microstructure characterization to elucidate the polymer chain length dependence of electron transport in n-type semiconducting polymers, exemplified by a naphthalene diimide-biselenophene copolymer, PNDIBS. Both bulk electron mobility measured by the space—charge limited current method and field-effect electron mobility of PNDIBS and other n-type semiconducting copolymers exhibit a peak at a critical degree of polymerization (DP_c) of 45–60 repeat units. The decreased electron mobility below DP_c is shown to originate from reduced intercrystallite connectivity while above DP_c intrachain twisting/folding, interchain entanglements, and intracrystallite limitations dominate electron transport. These findings provide a unified picture of the effects of



polymer molecular weight on electron transport in naphthalene diimide-based polymers and offer a more quantitative design rule for high-mobility n-type polymers with donor—acceptor architecture.

■ INTRODUCTION

Semiconducting polymers with good charge transport properties have paved the way for the rise of low-cost thin-film organic electronic devices, including organic field-effect transistors (OFETs), $^{1-6}$ organic light-emitting diodes (OLEDs) for commercial displays and lighting, organic solar cells (OSCs), $^{8-13}$ organic thermoelectrics (OTEs), $^{14-16}$ and bioelectronics. To Understanding of the structure–property relationships in semiconducting polymers has been essential to the design and synthesis of new materials with enhanced properties that advance these device applications. The charge carrier mobility (μ) of semiconducting polymers, in particular, is a key property that has been studied and substantially improved over the past two decades, leading to some polymers that now outperform polycrystalline silicon (μ > 10 cm²/V s). 3,5

Previous studies have demonstrated that high hole mobility can be achieved by increasing the polymer molecular weight (Figure S1a)^{20–24} in p-type semiconducting polymers such as regioregular poly(3-hexylthiophene) (P3HT) (Figure 1a), poly(dodecylquarterthiophene) (PQT) (Figure 1a), and poly(2,5-bis(3-alkylthiophen-2-yl)thieno-[3,2*b*]thiophene) (PBTTT) (Figure 1a). Recent studies of a broad range of polymer chain lengths in these p-type semiconducting polymers^{25–27} as well as other p-type polymers with polycyclic cores such as indacenodithiophene (IDTBT)^{28,29} and fluorene (F8BT)³⁰ have shown that the hole mobility reaches a

saturated value at a critical degree of polymerization ($\mathrm{DP_c}$) and then levels off rather than continuously increase with increasing DP. In particular, the hole mobility was found to depend on intercrystallite connectivity for $\mathrm{DP} < \mathrm{DP_c}$ and local lattice disorder for $\mathrm{DP} \geq \mathrm{DP_c}^{25-28}$ As a result, the hole mobility increases steeply to its maximum value once sufficient intercrystallite connectivity is established and levels off since the local lattice disorder remains relatively constant (Figure S1a).

The synthesis and investigation of the charge transport properties of n-type semiconducting polymers have generally lagged behind those of p-type conjugated polymers. Nevertheless, high electron mobility ($\mu > 3 \text{ cm}^2/\text{V s}$) has been achieved in some classes of n-type semiconducting polymers. The most extensively studied n-type semiconducting polymers have a donor—acceptor architecture 35,36 as exemplified by various naphthalene diimide (NDI)-based copolymers. Although the influences of the polymer molecular weight on the blend morphology, blend photo-

Received: August 1, 2022 Revised: September 30, 2022 Published: October 18, 2022





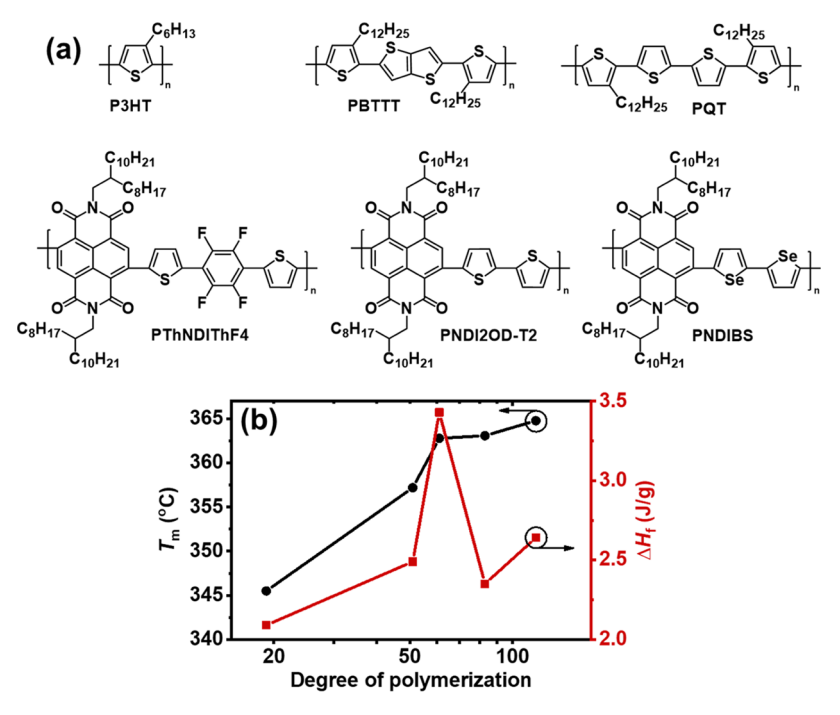


Figure 1. (a) Molecular structures of semicrystalline p-type semiconducting polymers (P3HT, PBTTT, and PQT) and weakly ordered n-type semiconducting polymers (PThNDIThF4, PNDI2OD-T2, and PNDIBS). (b) Degree of polymerization dependence of thermal properties of PNDIBS.

physics, and photovoltaic properties have been previously examined, ^{38–42} the dependence of electron mobility on polymer chain length and the physics governing electron transport in n-type semiconducting polymers remain scarcely explored.

Previous studies of polymer chain length effects on electron mobility in n-type conjugated polymers^{42–46} have shown different and even contradictory results (Figure S1b). For instance, a study of poly(naphthalene diimide-alt-bithiophene) (PNDI2OD-T2) (Figure 1a) showed that shorter polymer chain lengths facilitate improved electron mobility (Figure S1b) due to enhanced crystallinity. 44 However, this study did not specify whether the molecular weight was number-average or weight-average and how the molecular weight was characterized (solvent and temperature).⁴⁴ Additionally, the "higher crystallinity leads to higher mobility" rationalization is in disagreement with the current understanding that the lower molecular weight conjugated polymer with high degree of crystallinity exhibits lower carrier mobility due to defined grain boundaries acting as charge trapping sites. 20,45 A different study of the same PNDI2OD-T2 polymer has similarly reported that the polymer with lower molecular weight had enhanced electron mobility compared to the higher molecular weight ones (Figure S1b).45 We note that this study has overlooked the impacts of polydispersity index (PDI), which increased with increasing polymer molecular weight, where the PDI of the highest M_n sample (PDI = 3.0) was twice that of the lowest M_p sample (PDI = 1.40); thus, the observed increasing mobility with decreasing molecular weight might have been influenced by the lower PDI values. A recent study has tried to delineate the effects of PDI and M_n on the electron mobility of PNDI2OD-T2 by ensuring relatively narrow molecular weight distributions (PDI ~1.2 to 1.4) and found that the electron mobility increases with increasing polymer molecular weight (Figure S1b) due to the enhanced tie-chain

fraction. However, the PNDI2OD-T2 films were processed by drop-casting and subjected to solvent vapor annealing; thus, even though maximal chain alignment can be achieved, the observed electron mobility even at the highest molecular weight is much lower than the previously reported values (Figure S1b). On the other hand, another study reported that the electron mobility reached a peak at an optimal chain length (Figure S1b), which was attributed to an optimal degree of crystallinity. Furthermore, comprehensive understanding of molecular weight dependence of bulk electron transport in NDI-based n-type semiconducting polymers remains to be explored. In summary, the results of prior studies of effects of polymer chain length on electron mobility of n-type semiconducting polymers have been contradictory, and the offered explanations have been unsatisfactory.

In this paper, we report studies of the effects of polymer chain length DP on the electron transport and thin-film microstructure of poly(naphthalene diimide-alt-biselenophene) (PNDIBS) (Figure 1a), a model system for n-type semiconducting polymers with a donor-acceptor architecture. The series of PNDIBS samples, prepared via the direct hetero(arylation) polymerization (DHAP) method, had a sufficiently broad range of DP from 19 to 117. The fieldeffect electron mobility (μ_{OFET}) was measured using organic field-effect transistors (OFETs), and the bulk electron mobility (μ_{SCLC}) was measured via the space-charge limited current (SCLC) technique. We show that both μ_{OFET} and μ_{SCLC} of PNDIBS exhibit a peak at the same range of critical degree of polymerization (DP_c) of 45-60 repeat units. To facilitate connection of the macroscopic electron transport to the thinfilm microstructure of PNDIBS, we combined atomic force microscopy (AFM) imaging and 2D grazing incidence wideangle X-ray scattering (2D-GIWAXS) analyses to probe thinfilm multiscale polymer packings as a function of the chain length DP. We found that when DP is less than DP, the rate-

limiting step for efficient electron transport is intercrystallite transport due to insufficient electrical connectivity between ordered domains. In contrast, when DP is greater than DP_c, the rate-limiting step becomes intrachain, interchain, and intracrystallite transport due to backbone twisting, chain entanglements, and randomly distributed local fields acting as electron traps. Further analyses of paracrystallinity disorder, which is the local lattice disorder within a crystallite, along the polymer stacking in the lamellar and π - π stacking directions revealed the physical sources of local lattice disorder to be backbone twisting, chain folding and entanglement, and random sidechain conformational disorder. Available literature data on other NDI-based copolymers were found to also correspond to this unified picture of electron transport physics of this class of n-type semiconducting polymers.

EXPERIMENTAL METHODS

Materials. The synthesis and characterization of the series of PNDIBS samples of five different molecular weights, prepared using the DHAP method, have previously been reported by our groups.⁴¹

Characterization. The number-average (M_n) and weight-average (M_w) molecular weights were determined by size-exclusion chromatography (SEC) using high-temperature Varian Polymer Laboratories GPC220 equipped with an RI detector and a PL BV400 HT Bridge Viscometer. The column set consists of two PL gel Mixed C (300 × 7.5 mm²) columns and a PL gel Mixed C guard column. The flow rate was fixed at 1 mL/min using 1,2,4trichlorobenzene (TCB) (with 0.0125% w/v butylated hydroxytoluene (BHT) as an antioxidant) as the eluent. The temperature of the system was set at 110 °C. The samples (2 mg) were dissolved in 2 mL of TCB in 5 mL chromatography vials and then stirred and heated to 110 °C for 1 h for complete dissolution. Then, the polymer solution is filtered through a 0.45 μm cellulose fiber film into a 5 mL chromatography vial to ensure a homogeneous polymeric solution. The reported molecular weight data are based on polystyrene standards (Easi-Vials PS-M from Varian Polymer Laboratories) dissolved in TCB. Differential scanning calorimetry (DSC) analysis was performed on a TA Instrument Q100 under N2 flow by scanning from -10 to 400 °C at heating and cooling rates of 10 °C/min.

Fabrication and Characterization of OFETs at TAIWAN **TECH.** OFET devices were fabricated on highly doped n-type Si(100) wafers with a 300-nm-thick SiO₂ layer treated with a noctadecyltrimethoxysilane (OTMS) self-assembled monolayer according to the reported method.⁴⁷ Before use, the OTMS monolayer was rinsed sequentially with toluene, acetone, and isopropyl alcohol and dried under a N2 stream. Static water contact angles of the OTMS substrates were higher than 105° when measured using an Edmund Scientific goniometer. The solutions (5 mg/mL) of the polymer semiconductor for transistor devices were prepared by dissolving the polymer in chlorobenzene at 80 °C for 30 min and then spin-casted onto the OTMS-modified Si/SiO2 substrates with controlled thickness at ~40 nm. The as-prepared thin films were thermally annealed at 170 °C for 1 h in a N2-filled glovebox. Top-contact gold source/drain electrodes (70 nm) were subsequently deposited by evaporation through a shadow mask with the channel length (L) and width (W) defined as 50 and 1000 μ m, respectively. The transistor characteristics were measured using a Keithley 4200 semiconductor parameter analyzer (Keithley Instruments Inc., Cleveland, OH) in a N₂-filled glovebox at room temperature. The saturation region fieldeffect electron mobility, μ_{OFET} , was calculated from the standard FET relationship

$$I_{\rm ds} = \left(\frac{WC_{\rm i}}{2L}\right) (V_{\rm gs} - V_{\rm T})^2 \mu \tag{1}$$

Fabrication and Characterization of OFETs at the University of Washington. OFET devices were fabricated on heavily n-doped silicon (<0.005 Ω cm; 500 μ m) with a 300-nm-thick silicon dioxide layer. The surface of the cleaned substrate was treated with air plasma

before immersing in octadecyltrichlorosilane (OTS18):Toluene (1:500, v:v) overnight to form a self-assembled monolayer (SAM). Afterward, the treated substrates were washed and sonicated in toluene to remove excess physisorbed OTS-18, and then they were thermally annealed at 100 °C for 10 min in ambient air. Solutions of PNDIBS (5-7 mg/mL) were prepared by dissolving the polymer in chlorobenzene and stirred at 85 °C for at least 1 h inside a N2-filled glovebox. The PNDIBS solutions were spin-coated onto the OTS-18modified Si/SiO₂ substrates, and the resulting PNDIBS films were thermally annealed at 170 °C for 1 h in a N₂-filled glovebox. Source and drain electrodes were defined by thermal evaporation of gold (60 nm). The channel length (L) and width (W) were 100 and 1000 μ m, respectively. The transistor characteristics were measured using a Keithley 4200 SCS semiconductor parameter analyzer (Keithley Instruments Inc., Cleveland, OH) in a N2-filled glovebox at room temperature. The saturation region field-effect electron mobility, μ_{OFET} , was calculated from the standard FET relationship (eq 1).

Fabrication and Characterization of SCLC Devices. Current-voltage (J-V) characteristics of the SCLC devices were measured using a HP4155A semiconductor parameter analyzer (Yokogawa Hewlett-Packard, Tokyo). The carrier mobility was deduced by fitting the J-V curves to the Mott–Gurney equation where J is the current density, $\varepsilon_{\rm o}$ is the permittivity of free space, ε is the relative permittivity, $\mu_{\rm SCLC}$ is the zero-field mobility, V is the voltage, and L is the thickness of the semiconducting polymer layer

$$J = \frac{9}{8} \varepsilon_0 \varepsilon \mu \frac{V^2}{L^3} \tag{2}$$

The SCLC device structure was ITO/ZnO/PEI/PNDIBS/LiF (1 nm)/Al (100 nm). ZnO and polyethyleneimine (PEI) solutions were prepared as previously reported. 48,49 The ZnO precursor solution was spin-coated onto ITO substrates and annealed at 200 °C for 30 min in ambient air. Afterward, the PEI solution was spin-coated onto the dried ZnO layer and thermally annealed at 120 °C for 10 min. The ITO/ZnO/PEI-coated substrates were then transferred to an argon-filled glovebox to deposit the polymer semiconductor layer. The PNDIBS film was spin-coated at 1000 rpm for 50 s, followed by thermal annealing at 110 °C for 10 min inside an argon-filled glovebox.

AFM Imaging. Atomic force microscopy (AFM) characterization of the surface morphology of the PNDIBS films was done using a Bruker Dimension scanning probe microscope (SPM) system. Films of PNDIBS of different number-average molecular weight values were spin-coated at 1000 rpm for 50 s, followed by thermal annealing at 110 °C for 10 min inside an argon-filled glovebox.

GIWAXS. Grazing incidence X-ray scattering (GIWAXS) experiments were conducted at the Japan Synchrotron Radiation Facility SPring-8 using the beamlines BL46XU. Thin-film samples of PNDIBS were spin-coated on the top of glass substrates and annealed at 110 °C for 10 min. The X-ray beam was monochromatized by a doublecrystal Si(111) monochromator, and the X-ray energy in this experiment was 12.40 keV (λ = 0.1 nm). The angle of incident Xray to the sample surface was 0.12° with a Huber diffractometer. The scattered profile from the film sample was detected using an area detector (PILATUS 300 K) for 1 s at room temperature, and the distance between the sample and the detector was 175.0 mm. The crystal coherence length (L_c) of samples was determined using the Scherrer equation: $L_c = 2\pi K/\Delta q$, where K is a shape factor (typically 0.9) and $\hat{\Delta}q$ is the full width at half-maximum (FWHM) of the diffraction peak. Here, the L_c (100) and L_c (010) were, respectively, obtained from the FWHM of the (100) diffraction peak in the inplane (q_{xy}) line-cut and the FWHM of the (010) diffraction peak in the out-of-plane (q_z) line-cut.

■ RESULTS AND DISCUSSION

Optical and Thermal Properties. Thin-film optical absorption spectra of PNDIBS of various number-average molecular weight (M_n) values have been previously reported

by our group. 40,41 Two absorption bands centered at 397–399 and 711–718 nm were observed (Figure S2a), which are assigned to the π – π * transition and intramolecular charge transfer (ICT). 41 The main effect of $M_{\rm n}$ is a small progressive blue shift of the ICT band from 718 to 711 nm with increasing $M_{\rm n}$, with the exception of the 90 kDa sample, indicating that the intramolecular charge transfer interaction between the NDI moiety and the biselenophene moiety is weakened due to backbone distortion. 41 The slight bathochromic shift in the ICT band of the 90 kDa films suggests significant chain aggregation, which might be caused by the slightly higher PDI value (Table 1) compared to the other polymer samples.

Table 1. Molecular Weight, Optical Properties, and Thermal Properties of PNDIBS

$M_{\rm n}$ (kDa)	PDI	DP ^a	$\binom{T_{\mathrm{m}}}{(^{\circ}\mathrm{C})}$	$T_{\rm c}$ (°C)	$\frac{\Delta H_{\mathrm{f}}^{b}}{\left(\mathrm{J/g}\right)}$	(10^{-3} J/g K)
21	1.7	19.4	345.5	347.5	2.09	3.4
55	2.4	50.8	357.2	348.5	2.49	4.0
66	2.6	60.9	362.8	348.2	3.43	5.4
90	3.0	83.1	363.1	348.1	2.35	3.7
127	2.3	117.2	364.8	348.5	2.64	4.1

^aDP = $M_{\rm n}/M_{\rm s}$, where M is the molecular weight of a repeat unit. ^b $\Delta H_{\rm f}$ calculated from the differential scanning calorimetry (DSC) traces of the second cooling cycle. ^c $\Delta S_{\rm f}$ calculated from $\Delta S_{\rm f} = \Delta H_{\rm f}/T_{\rm m}$ assuming $\Delta G_{\rm f} = 0$ for equilibrium.

The polymer chain length dependence of the thermal properties of PNDIBS, as characterized by differential scanning calorimetry (DSC) scans (Figure S2b,c), including melting temperature (T_m) , crystallization temperature (T_c) , enthalpy of fusion (ΔH_f) , and entropy of fusion (ΔS_f) , are summarized in Table 1 and presented in Figure 1b. The $T_{\rm m}$ progressively increased from 345.5 °C at DP \sim 19 to 364.8 °C at DP \sim 117, which can be rationalized by increased chain folding and chain entanglements at the higher DP. 43,45 In contrast, the crystallization temperature T_c remained relatively constant at around 347.5-348.5 °C for DP varying between 19 and 117 (Table 1). The independence of T_c on DP can be explained by supercooling effects as exemplified by the temperature offset between the $T_{\rm m}$ and $T_{\rm c}$ (2–16 K) and the vertical lines after nucleation in the cooling traces (Figure S2c). In this case, the polymers crystallize rapidly even at a slow cooling rate of 10 $^{\circ}$ C/min; thus, the T_{c} appeared independent of the DP. The enthalpy of fusion ΔH_f reached its peak value of 3.43 J/g at DP \sim 60 and subsequently decreased as DP increased further. The entropy of fusion ΔS_f followed a similar DP dependence as ΔH_{θ} reaching a maximum at DP ~ 60 (Table 1). Since the change in entropy of fusion can be expressed as

 $\Delta S_{\rm f} = S_{\rm melt} - S_{\rm crystal} = k(\ln \Omega_{\rm melt} - \ln \Omega_{\rm crystal})$ (3)

where k is the Boltzmann constant and Ω_i is the total possible microscopic configurations of the polymer chains in state i, the observed maximum $\Delta S_{\rm f}$ at DP \sim 60 implies that $S_{\rm crystal}$ and $\Omega_{\rm crystal}$ are minimized and thus suggests highly ordered crystallites that enable efficient intrachain and interchain packings.

Field-Effect Electron Transport. We characterized the field-effect electron transport properties of several PNDIBS samples with different DP values using n-channel organic fieldeffect transistor (OFET) devices fabricated and characterized independently at the University of Science and Technology (TAIWAN TECH) and the University of Washington (UW). The TAIWAN TECH devices were fabricated using a bottomgate/top-contact architecture with channel dimensions of 50/ 1000 μ m (L/W), while the UW devices were fabricated using a bottom-gate/top-contact architecture with channel dimensions of $100/1000 \, \mu \text{m} \, (L/W)$. The output curves and transfer curves for the TAIWAN TECH devices are given in Figures S3 and S4, respectively, while those of the UW devices are presented in Figures S5 and S6. The OFET parameters for all devices are shown in Table 2. The saturated field-effect electron mobility (μ_{OFET}) as a function of DP is presented in Figure 2a. The on/ off current ratio $(I_{\rm on}/I_{\rm off})$ of the devices was generally very high $(>10^4-10^6)$ for all of the DP values. The average electron mobility μ_{OFET} obtained from the TAIWAN TECH devices increased from 0.16 cm $^2/V$ s at DP \sim 19 to a peak of 0.26 cm^2/V s at DP ~ 50 and subsequently decreased to 0.08 cm²/ V s at DP \sim 117. A similar trend in the μ_{OFET} as a function of DP was also observed for the UW devices where μ_{OFET} increased from 0.034 cm²/V s at DP \sim 19 to a maximum of $0.20 \text{ cm}^2/\text{V}$ s at DP $\sim 60 \text{ and dropped to } 0.07 \text{ cm}^2/\text{V}$ s at DP \sim 117. The slight difference in the absolute μ_{OFET} values obtained by the two institutions likely originated from the subtle differences in device fabrication procedures. Nevertheless, these results suggest that there exists a critical degree of polymerization (DP_c) range between 50 and 60 repeat units where the field-effect electron mobility is maximized. The observation of an increase in electron mobility of PNDIBS with chain length to a peak value followed by decrease past the DP_c regime is interesting and to be contrasted with the known chain length dependence of the hole transport properties of classic semicrystalline p-type semiconducting polymers, where the hole mobility does not decrease from its peak value (Figure S1a).²⁵⁻³⁰

Bulk Electron Transport. Toward a broader understanding of the chain length dependence of electron transport in PNDIBS, we next focused on using the space—charge limited current (SCLC) method to characterize the bulk electron transport in the films. Unlike OFET-derived electron

Table 2. Electron Transport Properties of PNDIBS

$M_{\rm n}$ (kDa)	DP	$\mu_{\rm SCLC}^{a} \left(10^{-4} \text{ cm}^2/\text{V s}\right)$	$\mu_{\text{FET}}^{}}}\text{EET$	$I_{\rm on}/I_{\rm off}^{b}$	$V_{t}^{\boldsymbol{b}}$ (V)	$\mu_{\rm FET}^{\ c} \left({\rm cm}^2/{\rm V} \ {\rm s}\right)$	$I_{\rm on}/I_{\rm off}{}^c$	$V_{t}^{c}\left(V\right)$
21	19.4	1.68 ± 0.42	0.034 ± 0.006	>10 ⁵	11.7	0.16 ± 0.003	>10 ⁶	27.6
55	50.8	3.89 ± 0.97	0.15 ± 0.03	>10 ⁵	14.6	0.26 ± 0.05	>106	29.0
66	60.9	4.91 ± 0.63	0.20 ± 0.06	>10 ⁵	15.5	0.23 ± 0.05	>106	31.2
90	83.1	1.22 ± 1.50	0.10 ± 0.03	>104	5.9	0.20 ± 0.01	>106	27.5
127	117.2	0.91 ± 0.31	0.07 ± 0.01	>104	4.3	0.08 ± 0.02	>106	23.9

[&]quot;Average values were obtained from four different devices. bAverage values were obtained from at least six different devices, which were fabricated and characterized at the UW. Average values were obtained from six different devices, which were fabricated and characterized at TAIWAN TECH.

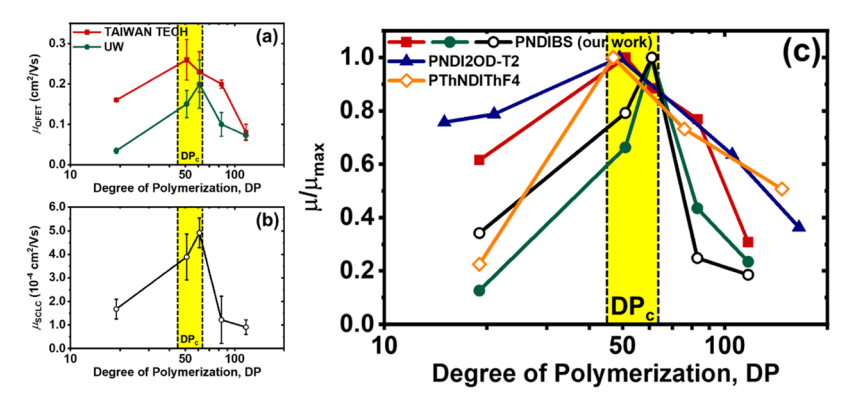


Figure 2. (a) Dependence of field-effect electron mobility (μ_{OFET}) on the degree of polymerization of PNDIBS for devices fabricated independently at TAIWAN TECH and at the UW. Error bars represent \pm standard deviation. (b) Dependence of bulk electron mobility (μ_{SCLC}) on the degree of polymerization of PNDIBS. Error bars represent \pm standard deviation. (c) Normalized (μ/μ_{max}) field-effect electron mobility (filled symbols) and bulk electron mobility (unfilled symbols) as a function of the degree of polymerization of n-type semiconducting polymers including our present work and literature data.

mobility μ_{OFET} , which is sensitive to only a few nanometers of the semiconductor near the dielectric interface, the SCLC electron mobility (μ_{SCLC}) characterizes the bulk electron mobility over a few hundred nanometers of the semiconductor layer sandwiched between the electrodes. Details of the fabrication and characterization procedures for the electrononly SCLC devices, ITO/ZnO/PEI/PNDIBS/LiF/Al, are outlined in the Experimental Methods. The SCLC *I–V* curves and the Mott-Gurney equation fit lines are given in Figure S7, and the average SCLC electron mobility values are summarized in Table 2. The dependence of the bulk electron mobility μ_{SCLC} on the degree of polymerization is shown in Figure 2b. The average electron mobility increases monotonically from $1.68 \times 10^{-4} \text{ cm}^2/\text{V}$ s to a peak at $4.91 \times 10^{-4} \text{ cm}^2/\text{V}$ s as the polymer chain elongates from around 20 repeat units to around 50-60 repeat units beyond which the μ_{SCLC} value steeply decreases to 0.91×10^{-4} cm²/V s (Table 2). This result indicates that there is also a critical polymer chain length region between 50 and 60 repeat units where the bulk electron mobility is maximized. The fact that both the field-effect electron mobility and the bulk electron mobility are maximized at the same DP_c range between 50 and 60 repeat units for PNDIBS is very significant since this has not been previously identified in the literature.

To arrive at a more complete understanding of the physics of electron transport in n-type semiconducting polymers, we collected a few available literature data on polymer molecular weight dependence of electron mobility, 42,43 where the conjugated polymers were processed from the common solvent (chlorobenzene or chloroform) and deposition methods (i.e., spin-coating), and the polymer molecular weights were characterized at high temperature $(T > 80 \, ^{\circ}\text{C})$. The normalized electron mobility (μ/μ_{max}) as a function of the degree of polymerization DP for the present PNDIBS along with the literature data for various naphthalene diimide (NDI)based conjugated polymers are shown in Figure 2c. It is clear from the data in Figure 2c that the maximum electron mobility is observed in a narrow range of critical degree of polymerization of about 45-60 repeat units for all of the polymers, suggesting generality of the observed dependence of electron transport on polymer molecular weight beyond PNDIBS.

The observed peak in the dependence of *electron* mobility on DP of n-type semiconducting polymers is in sharp contrast

with the known chain length dependence of hole mobility of ptype semiconducting polymers, where the hole mobility saturates and levels off once interdomain connectivity is established (Figure S1a). What this difference in DP dependence suggests is that factors limiting efficient electron transport in n-type semiconducting polymers are different from those limiting hole transport in p-type semiconducting polymers.^{25–30} Furthermore, we note that the different NDIbased n-type semiconducting polymers, whose electron transport data in Figure 2c show similar trend, have a donor-acceptor architecture with very different donor moieties; this implies that the physics governing multiscale electron transport is universal across at least this class of n-type semiconducting polymers. Thus, to elucidate the underlying mechanisms governing the chain length dependence of electron transport properties in the class of NDI-based ntype semiconducting polymers, we sought to understand the morphology of PNDIBS thin films using AFM and GIWAXS characterization results presented below.

Surface Morphology. AFM height images of PNDIBS thin films are shown in Figure S8, and the calculated twodimensional fast Fourier transformed (2D-FFT) images are presented in Figure S9. Thin films of PNDIBS within the DP_c range exhibited highly ordered and elongated fibrillar structures (Figure S8b,c), whereas films of PNDIBS outside the DP_c range were featureless (Figure S8a,d,e). Moreover, the root-mean-square surface roughness (R_a) of films within the DP_c range was found to be the smallest $(R_q = 0.68-0.72 \text{ nm})$, suggesting a homogeneous and well-connected network of crystalline domains. Further examination of the orientational alignment of the fibrils by 2D-FFT images showed that samples where DP is higher than DP, exhibited a uniform radial distribution (Figure S9d,e), indicating that the fibrils are randomly oriented with no preferential directionality across the film surfaces. 45,50 In contrast, samples where DP \leq DP_c showed anisotropic 2D-FFT images (Figure S9a-c), which suggests strong fiber alignment along certain directions over several micrometers 45,50 and thus very surprising since the films were prepared by spin-coating and not by any processing technique that could induce preferential orientation (e.g., blade coating, solution shearing, or inkjet printing). The presence of strong fibrillar directionality in the thin-film microstructure of PNDIBS in the DP_c range is expected to be beneficial to the

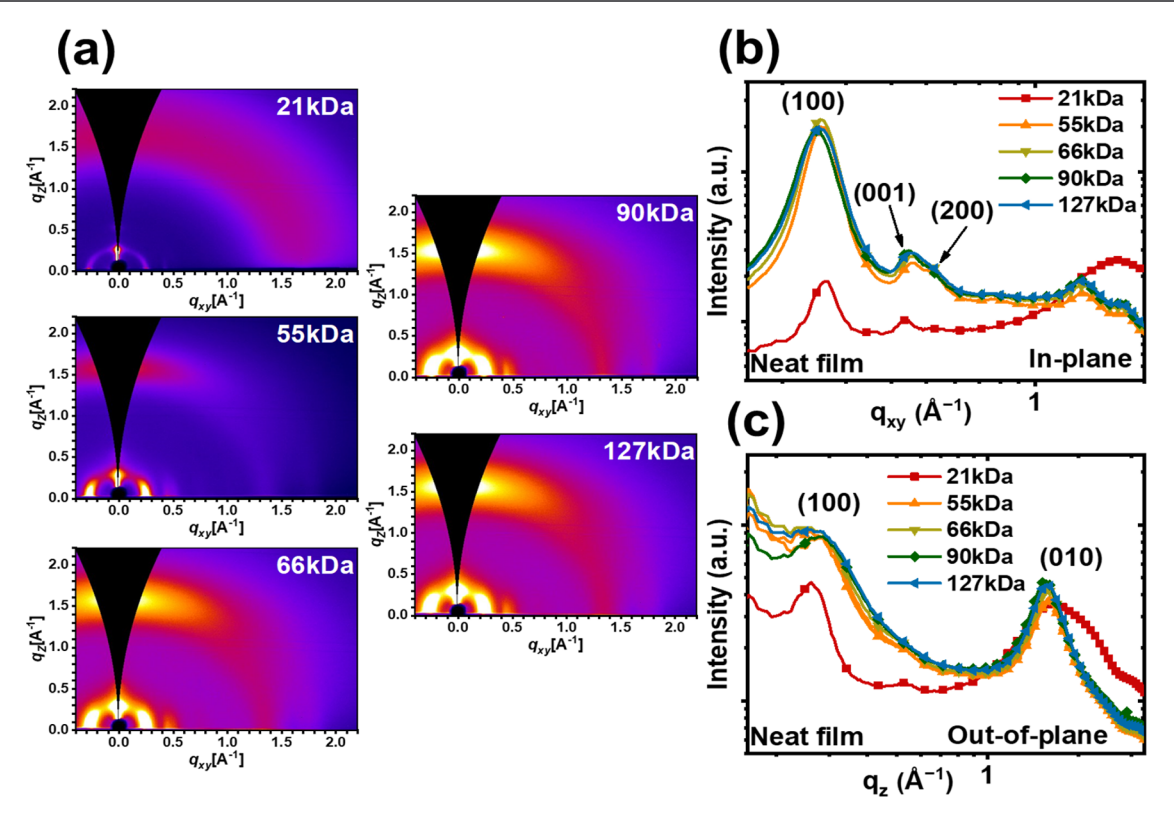


Figure 3. Molecular weight dependence of 2D-GIWAXS data for PNDIBS thin films: (a) 2D-GIWAXS patterns; (b, c) 1D line-cuts of GIWAXS patterns in the in-plane (IP) direction (b) and the out-of-plane (OOP) direction (c).

Table 3. Summary of Lamellar d-Spacing Distance, $\pi-\pi$ Stacking Distance, Crystalline Coherence Length (L_c) in the In-Plane (IP) and Out-of-Plane (OOP) Directions, and the Paracrystallinity Disorder in the Lamellar (g_{lam}) and π -Stacking Directions (g_{π}) of PNDIBS Films at Various Number-Average Molecular Weight (M_n) Values

$M_{\rm n}~({ m kDa})$	DP	d-spacing (Å)	π – π distance (Å)	$L_{\rm c} \ ({\rm nm}) \ (100) \ {\rm IP}$	$L_{\rm c}$ (nm) (010) OOP	g _{lam} (%) (100) IP	g_{π} (%) (010) OOP
21	19.4	23.5	3.83	14.0	0.54	15.7	30.9
55	50.8	24.7	3.94	11.4	1.24	17.5	21.4
66	60.9	24.7	3.96	10.7	1.26	18.2	21.2
90	83.1	25.3	4.06	9.6	1.36	19.4	20.6
127	117.2	24.7	4.00	9.3	1.30	19.5	20.9

multiscale electron transport properties as further discussed below.

Bulk Thin-Film Morphology. Two-dimensional grazing incidence wide-angle X-ray scattering (2D-GIWAXS) measurements were carried out on thin films of PNDIBS of various molecular weights. The 2D-GIWAXS images and the 1D linecuts for PNDIBS films are presented in Figure 3. The peak positions are summarized in Table S1, whereas the lamellar spacings, the $\pi-\pi$ stacking distance, the crystalline coherence length (L_c) , and the paracrystallinity disorder (g) are presented in Table 3.

The film of PNDIBS of various molecular weights had an intense (100) diffraction peak in the in-plane (IP) direction at $q_{xy} = 0.25-0.27 \text{ Å}^{-1}$ (Table S1), which corresponds to varying lamellar d-spacing of 23.5–25.3 Å (Table 3). These lamellar packing distances in PNDIBS films are significantly shorter than expected from their alkyl chain lengths, which is indicative of strong interdigitation of the alkyl side chains between adjacent polymer backbones. Except for the lowest molecular weight sample ($M_{\rm n} = 21 \text{ kDa}$), films of the higher molecular weight PNDIBS also exhibited higher order diffraction peaks (h00) in the in-plane direction (Figure 3b). In the out-of-plane

(OOP) direction, the PNDIBS-21 kDa thin films showed a distinct (100) peak and a very broad (010) peak at q_z of 0.26 and 1.64 Å⁻¹, respectively, suggesting that the low molecular weight PNDIBS adopts both edge-on and face-on molecular orientations. Films of all of the higher molecular weight PNDIBS samples exhibited a sharp and intense (010) diffraction peak at $q_z = 1.55-1.59$ Å⁻¹ (Table S1) accompanied by a broad and weak (100) peak in the OOP direction, which suggests that most of the crystallites were oriented face-on with respect to the substrates. The $\pi-\pi$ stacking distances in the PNDIBS thin films of various M_n values are found to be 3.83–4.06 Å (Table 3), which are comparable to previous reports of $\pi-\pi$ stacking distances in majority of NDI-based semiconducting copolymers.⁵¹

An interesting visualization of how the thin-film microstructure evolves as a function of the polymer chain length is obtained in Figure 4 by displaying the dependence of the lamellar d-spacing and $\pi - \pi$ stacking distance versus the degree of polymerization DP (Figure 4a). Three distinct regions, including DP < DP_c, DP = DP_c, and DP > DP_c, can be identified, each of which represents a specific polymer packing motif as illustrated in Figure 4b. In region I (DP < DP_c), the

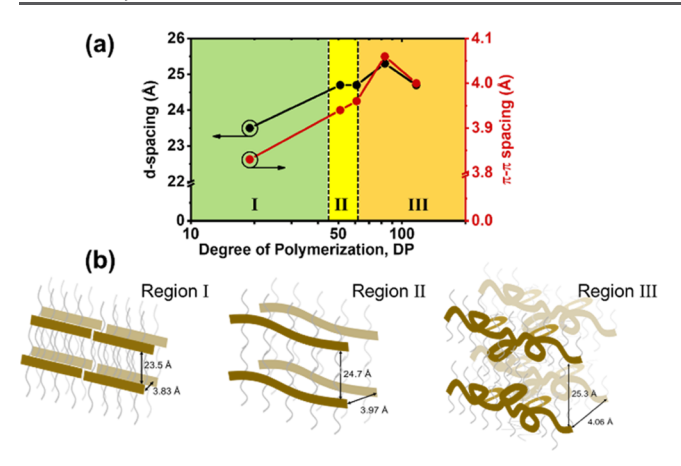


Figure 4. (a) Effects of degree of polymerization on the intermolecular packing distances in the lamellar direction (d-spacings) and π -direction (π - π spacings) and (b) schematic of the solid-state packings as a function of polymer chain length.

shortest d-spacing and π - π stacking distances indicate that these short polymer chains are packed efficiently, featuring high backbone planarity and improved intermolecular π orbital overlapping.⁵² In region II (DP = DP_c), both the lamellar distance and the π - π stacking distance increase, which can be seen as consequences of some degree of backbone twisting. In region III (DP > DP_c), further increases in the lamellar distance and the π -stacking distance are observed, suggesting significant chain folding, chain entanglements, and random rotational conformation of the flexible alkyl side chains. We note that the slightly higher lamellar and $\pi - \pi$ stacking distance observed in the 90 kDa sample compared to the 127 kDa sample could be due to increased chain aggregation as evidenced by the previously discussed bathochromic shift in the optical absorption. Nevertheless, the proposed microstructural pictures (Figure 4b) are well corroborated by the optical and thermal properties as well as the paracrystallinity disorder as discussed below. We also note that our proposed evolution of thin-film microstructures as a function of polymer chain length is in good accordance with a study on diketopyrrolopyrrole (DPP)-based semiconducting polymers.⁵³ Clearly, the observed evolution of intramolecular and intermolecular packings as a function of chain length can significantly influence the multiscale electron transport in PNDIBS films as further discussed below.

The crystalline coherence length (L_c) values estimated from the full width at half-maxima of both the (100) diffraction peak in the IP direction and the (010) diffraction peak in the OOP direction are presented in Table 3, while the chain length dependence of L_c values is shown in Figure 5a. The IP direction L_c (100) value is found to monotonically decrease with increasing degree of polymerization from 14.0 nm at DP \sim 19 to 9.3 nm at DP \sim 117, which means that the crystallite sizes and the crystallinity progressively decrease as the polymer chain grows. In addition, the OOP direction L_c (010) value increases with increasing chain length (Figure 5a) from 0.54 nm (DP \sim 19) to 1.24–1.26 nm (DP \sim 60) and to 1.30–1.36 nm (DP > 80). The observed progressive increase in the values of L_c (010) suggests slightly enhanced long-range ordering as the polymer chain grows. ⁵⁴

The paracrystallinity disorder was also estimated using the single-peak fit approximation method^{25,55} in both the lamellar direction (g_{lam}) and the π -stacking direction (g_{π}) to quantify

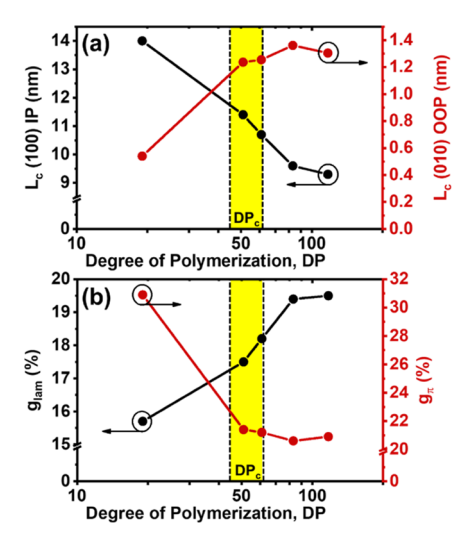


Figure 5. (a) Effects of polymer chain length on crystalline coherence length (L_c) and (b) effects of polymer chain length on paracrystallinity disorder (g).

the degree of intracrystallite disorder. The numerical values of g_{lam} and g_{π} are summarized in Table 3, while the relationships between the degree of polymerization and g values are shown in Figure 5b. With the exception of the lowest molecular weight sample (DP \sim 19) where g_{π} is likely to be overestimated due to the extremely broad (010) diffraction peak in the OOP direction (Figure 3c), the g_{π} values of the other samples remain constant at around 21%. This result implies that the local disorder within a crystallite along the π stacking direction is independent of the polymer chain length. On the other hand, the g_{lam} values are found to gradually increase with increasing degree of polymerization from around 16% (DP \sim 19) to 18% (DP \sim 60) and to 20% (DP > 80). This observation suggests that the physical source of local lattice disorder of n-type semiconducting polymers, which has remained unclear thus far,⁵⁶ lies in chain folding, kinks, and random side-chain entanglements, which can be worsened at longer polymer chain lengths. The increasing disorders in the lamellar direction could significantly disrupt efficient stackings and render the polymer more amorphous, which further corroborates the proposed microstructural pictures (Figure 4b) and is in good agreement with the observed trend in the IP direction L_c (100) values.

Understanding Electron Transport in n-Type Semi**conducting Polymers.** The key experimental observations on the electron transport properties and the thin-film morphology of PNDIBS can be summarized as follows: (i) both the field-effect electron mobility and bulk electron mobility are found to be concurrently maximized at a critical range of polymer chain length DP_c of 45-60 repeat units. This important structure-property relationship finding for NDIbased semiconducting polymers is likely to be broadly applicable to other classes of n-type D-A copolymers; (ii) preferential alignment of fibrils over several micrometers across the film surface is observed for $DP \leq DP_c$; (iii) three distinct microstructure regimes, DP < DP_{ct}, DP = DP_{ct}, and DP > DP_{ct} were found to characterize the evolution of the lamellar distance and the π - π stacking distance as a function of polymer chain length; (iv) the polymer crystallinity decreases monotonically with increasing polymer chain length; and (v) the paracrystallinity disorder in the π -stacking direction is

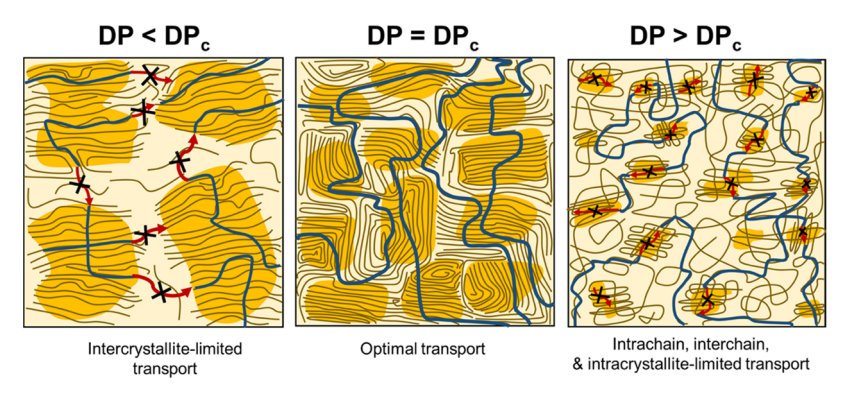


Figure 6. Schematic of the proposed picture of how polymer chain length influences macroscopic charge transport in n-type semiconducting polymers.

independent of the polymer chain length, whereas the paracrystallinity disorder in the lamellar direction scales approximately linearly with the polymer chain length.

Increasing the polymer molecular weight to maximize the crystallinity is one of the longstanding material design rules for achieving efficient charge transport in conjugated polymers. ^{4,22,57} However, our results in conjunction with available literature data show that there is rather a weak correlation between the crystallite size and electron mobility in NDI-based n-type semiconducting polymers (Figure S10). This finding suggests that there are other factors, beyond material crystallinity and maximal polymer chain length, that hinder efficient macroscopic electron transport in NDI-based n-type semiconducting polymers.

Based on the above results on polymer chain-length-dependent electron transport properties and thin-film microstructure results from AFM imaging and 2D-GIWAXS analyses, we propose a schematic to visualize the multiscale packing of polymers as a function of the chain length (Figure 6). We use the schematic in Figure 6 to guide the delineation of various factors that limit electron transport in PDNIBS and other n-type semiconducting polymers. The overall macroscopic electron mobility can be expressed as the sum of a series of mobilities spanning over multiscale 59,60 from intrachain ($\mu_{\text{intrachain}}$) and interchain ($\mu_{\text{interchain}}$) to intracrystallite ($\mu_{\text{intracrystallite}}$) and intercrystallite ($\mu_{\text{intercrystallite}}$)

$$\frac{1}{\mu} = \frac{1}{\mu_{\rm intrachain}} + \frac{1}{\mu_{\rm interchain}} + \frac{1}{\mu_{\rm intracrystallite}} + \frac{1}{\mu_{\rm intercrystallite}}$$
(4)

In the case of DP < DP $_{c}$, the polymer chains are the least coiled, ensuring maximum backbone planarity and thus enabling efficient intrachain mobility. Moreover, polymer chains in this regime also exhibit shorter intermolecular packing distances in the π -stacking direction, as described earlier, leading to improved interchain electronic coupling and increased electron hopping rate and thus overall enhanced interchain mobility. However, the short polymer chain length severely limits electron transport between crystallites due to insufficient intercrystallite connectivity, thus inhibiting the intercrystallite mobility. As a result, the DP < DP $_{c}$ regime is characterized by intercrystallite-limited electron transport (Figure 6)

$$\frac{1}{\mu} \sim \frac{1}{\mu_{\rm intercrystallite}}$$
, for DP < DP_c (5)

In the case of DP > DP_{ct} the intercrystallite transport is no longer the rate-limting step since sufficient electrical connectivity can be provided by the much longer polymer chains. The above 2D-GIWAXS results revealed that although the paracrystallinity disorder in the π - π direction remained relatively constant, the paracrystallinity disorder along the lamellar direction increased dramatically in the longer polymer chains due to intrachain folding, interchain entanglements, and random conformational disorder of the flexible alkyl side chains, thereby reducing intracrystallite ordering. Severe chain folding and chain entanglements also result in inefficient intermolecular packing featuring larger π – π stacking distances and consequently diminished short-range ordering and hindered intrachain charge delocalization and interchain hopping rate. Furthermore, the lack of a preferential fibrillar directionality suggests that the long polymer chains are likely to be randomly oriented across the film surface. Consequently, intrinsic dipole moments of the polymer chains can act as random local fields that trap electrons and significantly reduce the mobility. 61 Thus, the DP > DP_c regime can be categorized as intrachain, interchain, and intracrystallite-limited electron transport (Figure 6)

$$\begin{split} \frac{1}{\mu} \sim \frac{1}{\mu_{\text{intrachain}}} + \frac{1}{\mu_{\text{interchain}}} + \frac{1}{\mu_{\text{intracrystallite}}}, \\ \text{for DP} > \text{DP}_c \end{split} \tag{6}$$

In the critical chain length range, $DP = DP_c$, sufficient intercrystallite connectivity, efficient intrachain electron delocalization, fast interchain hopping rate, combined with strong fiber alignment across several micrometers of the film surface facilitate maximal electron transport (Figure 6). Thus, in this critical degree of polymerization range, the electron mobility is best described by eq 4.

The reason why the dependence of charge transport on polymer molecular weight in n-type polymers intrinsically differs from that of p-type polymers is likely to originate from the polymer architectures. The trend of hole mobility as a function of DP in p-type polymers has been reported mostly for either semicrystalline homopolymers (P3HT, PBTTT, and PQT)^{20–25,62} or donor—acceptor polymers with polycyclic cores (indacenodithiophene and fluorene).^{28–30} These p-type polymers bear linear alkyl side chains, which allow for better interdigitation, efficient packing, and more resistance to entanglement as evidenced by the relatively constant structural disorder, ^{25–28,30} implying that once sufficient intercrystallite connectivity is achieved, the hole mobility in p-type polymers

remains relatively constant. We speculate that if bulky and branch side chains were incorporated into p-type polymers instead of linear chains, increased structural disorder would be inevitable. In that case, the chain length dependence of hole mobility would likely be similar to the observed trend in our present study, that is, μ_h would increase to a maximum value representing intercrystallite-limited transport regime and subsequently decrease, signifying intrachain-, interchain-, and intracrystallite-limited transport regimes. Indeed, a recent study of DPP-based semiconducting polymers bearing 4hexyldodecyl side chains shows that the hole mobility is optimized at an intermediate molecular weight.⁵³ On the other hand, a common design motif for not only NDI-based polymers but also other high-performing n-type polymers is the donor-acceptor architecture with large branched alkyl side chains for sufficient solubility. The long alkyl chains are susceptible to entanglement, and significant backbone torsional disorder can be expected between the donor moiety and the acceptor moiety causing chain folding/kinks. As a result, maximum electron mobility can only be observed within the DP_c regime where intrachain mobility, interchain mobility, intracrystallite mobility, and intercrystallite mobility are simultaneously optimized.

Additional future studies of other classes of n-type semiconducting polymers with donor—acceptor architectures are needed to strengthen this picture of electron transport in n-type semiconducting polymers. Nevertheless, we believe that the present results and analyses provide a foundation for understanding of electron transport in PNDIBS and other n-type semiconducting polymers. A new guide to materials design toward high electron mobility n-type conjugated polymers that emerges from this unified understanding is that rather than aiming to maximize molecular weight and crystallinity *per se*, the goal should be to achieve a polymer molecular weight in the critical range (DP = DP_c), which globally optimizes contributions from intrachain, interchain, intracrystallite, and intercrystallite transport.

CONCLUSIONS

In conclusion, we have used the donor-acceptor copolymer PNDIBS as a model system to investigate the polymer chain length dependence of electron transport in naphthalene diimide-based n-type semiconducting polymers. We found that both the field-effect electron mobility and the bulk electron mobility measured by the SCLC technique are maximized within the same range of critical polymer chain length (DP_c) of 45-60 repeat units of PNDIBS and other NDI-based n-type semiconducting polymers. A parallel characterization of the thin-film microstructure evolution with PNDIBS degree of polymerization by AFM and GIWAXS analyses has enabled a mechanistic understanding of the observed electron mobility dependence on DP. Thus, outside of the critical polymer chain length range, the decreased electron transport is shown to arise from intercrystallite limitations for DP < DPc, whereas intrachain, interchain, and intracrystallite transport constrained electron mobility for DP $> DP_c$.

The present results also suggest that unlike longstanding understanding of the critical role of maximal crystallinity on the hole mobility of poly(3-hexylthiophene) and other p-type semiconducting polymers, electron transport in n-type semiconducting polymers is only weakly correlated with crystallinity. The distinct behaviors of the paracrystallinity disorder

along the lamellar and π – π stacking directions have facilitated unmasking of the physical sources of local lattice disorder in this series of PNDIBS to be random side-chain conformational disorder, chain folding, and chain entanglements. Finally, we highlight a guide to materials design toward high electron mobility n-type conjugated polymers that emerges from our present results: It is that rather than aiming to maximize molecular weight and crystallinity *per se*, the goal should be to target a polymer molecular weight in the critical range (DP_c) since this can globally optimize contributions from intrachain, interchain, intracrystallite, and intercrystallite transport.

ASSOCIATED CONTENT

Supporting Information

The Supporting Information is available free of charge at https://pubs.acs.org/doi/10.1021/acs.chemmater.2c02357.

Additional characterization data: DSC scans, transfer curves of n-channel OFET devices, $J^{1/2}-V$ curves measured by the SCLC technique and the corresponding fits, AFM images and 2D-FFT analyses of polymer films, and 2D-GIWAXS diffraction peak positions (PDF)

AUTHOR INFORMATION

Corresponding Author

Samson A. Jenekhe — Department of Chemical Engineering and Department of Chemistry, University of Washington, Seattle, Washington 98195-1750, United States; orcid.org/0000-0002-0898-9541; Email: jenekhe@u.washington.edu

Authors

Duyen K. Tran — Department of Chemical Engineering and Department of Chemistry, University of Washington, Seattle, Washington 98195-1750, United States; orcid.org/0000-0002-3065-6153

Amélie Robitaille – Département de Chimie, Université Laval, Quebec City, Quebec G1V 0A6, Canada

I Jo Hai – Department of Chemical Engineering, National Taiwan University of Science and Technology (TAIWAN TECH), Taipei 106, Taiwan

Chia-Chun Lin – Department of Chemical Engineering, National Taiwan University of Science and Technology (TAIWAN TECH), Taipei 106, Taiwan

Daiki Kuzuhara — Faculty of Science and Engineering, Iwate University, Morioka, Iwata 020-8551, Japan; orcid.org/0000-0001-7948-8501

Tomoyuki Koganezawa – Industry Application Division, Japan Synchrotron Radiation Research Institute, Sayo, Hyogo 679-5198, Japan

Yu-Cheng Chiu — Department of Chemical Engineering, National Taiwan University of Science and Technology (TAIWAN TECH), Taipei 106, Taiwan; ⊚ orcid.org/ 0000-0003-4812-5681

Mario Leclerc — Département de Chimie, Université Laval, Quebec City, Quebec G1V 0A6, Canada; [®] orcid.org/0000-0003-2458-9633

Complete contact information is available at: https://pubs.acs.org/10.1021/acs.chemmater.2c02357

Author Contributions

The manuscript was written through contributions of all authors. All authors have given approval to the final version of the manuscript.

Notes

The authors declare no competing financial interest.

ACKNOWLEDGMENTS

This work was supported by the National Science Foundation (DMR-1708450 and DMR-2003518). Work at the Université Laval was supported by NSERC. Part of this work was conducted at the Molecular Analysis Facility, a National Nanotechnology Coordinated Infrastructure (NNCI) site at the University of Washington, which is supported in part by funds from the National Science Foundation via Awards NNCI-2025489 and NNCI-1542101, the Molecular Engineering and Sciences Institute, and the Clean Energy Institute. Synchrotron radiation-based 2D-GIWAXS experiments were performed at the BL46XU of SPring-8 with the support of the Japan Synchrotron Radiation Research Institute (JASRI) (Proposal Nos. 2018A1744, 2018B1772, 2021B1947, 2022A2063, and 2022A2069).

REFERENCES

- (1) Babel, A.; Jenekhe, S. A. High Electron Mobility in Ladder Polymer Field-Effect Transistors. *J. Am. Chem. Soc.* **2003**, *125*, 13656–13657.
- (2) Mei, J.; Diao, Y.; Appleton, A. L.; Fang, L.; Bao, Z. Integrated Materials Design of Organic Semiconductors for Field-Effect Transistors. *J. Am. Chem. Soc.* **2013**, *135*, 6724–6746.
- (3) Quinn, J. T. E.; Zhu, J.; Li, X.; Wang, J.; Li, Y. Recent progress in the development of n-type organic semiconductors for organic field effect transistors. *J. Mater. Chem. C* **2017**, *5*, 8654–8681.
- (4) Paterson, A. F.; Singh, S.; Fallon, K. J.; Hodsden, T.; Han, Y.; Schroeder, B. C.; Bronstein, H.; Heeney, M.; McCulloch, I.; Anthopoulos, T. D. Recent Progress in High-Mobility Organic Transistors: A Reality Check. *Adv. Mater.* **2018**, *30*, No. 1801079.
- (5) Kim, M.; Ryu, S. U.; Park, S. A.; Choi, K.; Kim, T.; Chung, D.; Park, T. Donor-Acceptor-Conjugated Polymer for High-Performance Organic Field-Effect Transistors: A Progress Report. *Adv. Funct. Mater.* **2019**, *30*, No. 1904545.
- (6) Fratini, S.; Nikolka, M.; Salleo, A.; Schweicher, G.; Sirringhaus, H. Charge transport in high-mobility conjugated polymers and molecular semiconductors. *Nat. Mater.* **2020**, *19*, 491–502.
- (7) Kulkarni, A. P.; Tonzola, C. J.; Babel, A.; Jenekhe, S. A. Electron Transport Materials for Organic Light-Emitting Diodes. *Chem. Mater.* **2004**, *16*, 4556–4573.
- (8) Lee, C.; Lee, S.; Kim, G.-U.; Lee, W.; Kim, B. J. Recent Advances, Design Guidelines, and Prospects of All-Polymer Solar Cells. *Chem. Rev.* **2019**, *119*, 8028–8086.
- (9) Genene, Z.; Mammo, W.; Wang, E.; Andersson, M. R. Recent Advances in n-Type Polymers for All-Polymer Solar Cells. *Adv. Mater.* **2019**, *31*, No. 1807275.
- (10) Earmme, T.; Hwang, Y.-J.; Murari, N. M.; Subramaniyan, S.; Jenekhe, S. A. All-Polymer Solar Cells with 3.3% Efficiency Based on Naphthalene Diimide-Selenophene Copolymer Acceptor. *J. Am. Chem. Soc.* **2013**, *135*, 14960–14963.
- (11) Hwang, Y.-J.; Courtright, B. A. E.; Ferreira, A. S.; Tolbert, S. H.; Jenekhe, S. A. 7.7% Efficient All-Polymer Solar Cells. *Adv. Mater.* **2015**, *27*, 4578–4584.
- (12) Hwang, Y.-J.; Earmme, T.; Courtright, B. A. E.; Eberle, F. N.; Jenekhe, S. A. n-Type Semiconducting Naphthalene Diimide-Perylene Diimide Copolymers: Controlling Crystallinity, Blend Morphology, and Compatibility Toward High-Performance All-Polymer Solar Cells. J. Am. Chem. Soc. 2015, 137, 4424—4434.

- (13) Jia, T.; Zhang, J.; Zhong, W.; Liang, Y.; Zhang, K.; Dong, S.; Ying, L.; Liu, F.; Wang, X.; Huang, F.; Cao, Y. 14.4% efficiency all-polymer solar cell with broad absorption and low energy loss enabled by a novel polymer acceptor. *Nano Energy* **2020**, *72*, No. 104718.
- (14) Lu, Y.; Wang, J.-Y.; Pei, J. Strategies To Enhance the Conductivity of n-Type Polymer Thermoelectric Materials. *Chem. Mater.* **2019**, *31*, 6412–6423.
- (15) Sun, Y.; Di, C.-A.; Xu, W.; Zhu, D. Advances in n-Type Organic Thermoelectric Materials and Devices. *Adv. Electron. Mater.* **2019**, *5*, No. 1800825.
- (16) Xu, K.; Sun, H.; Ruoko, T.-P.; Wang, G.; Kroon, R.; Kolhe, N. B.; Puttisong, Y.; Liu, X.; Fazzi, D.; Shibata, K.; Yang, C.-Y.; Sun, N.; Persson, G.; Yankovich, A. B.; Olsson, E.; Yoshida, H.; Chen, W. M.; Fahlman, M.; Kemerink, M.; Jenekhe, S. A.; Mueller, C.; Berggren, M.; Fabiano, S. Ground-state electron transfer in all-polymer donor-acceptor heterojunctions. *Nat. Mater.* **2020**, *19*, 738–744.
- (17) Rivnay, J.; Inal, S.; Salleo, A.; Owens, R. M.; Berggren, M.; Malliaras, G. G. Organic electrochemical transistors. *Nat. Rev. Mater.* **2018**, 3, 17086.
- (18) Paulsen, B. D.; Tybrandt, K.; Stavrinidou, E.; Rivnay, J. Organic mixed ionic—electronic conductors. *Nat. Mater.* **2020**, *19*, 13–26.
- (19) Sun, H.; Wang, L.; Wang, Y.; Guo, X. Imide-Functionalized Polymer Semiconductors. *Chem. Eur. J.* **2019**, *25*, 87–105.
- (20) Kline, R. J.; McGehee, M. D.; Kadnikova, E. N.; Liu, J.; Frechet, J. M. J. Controlling the Field-Effect Mobility of Regioregular Polythiophene by Changing the Molecular Weight. *Adv. Mater.* **2003**, *15*, 1519–1522.
- (21) Goh, C.; Kline, R. J.; McGehee, M. D.; Kadnikova, E. N.; Frechet, J. M. J. Molecular-weight-dependent mobilities in regioregular poly(3-hexyl-thiophene) diodes. *Appl. Phys. Lett.* **2005**, *86*, No. 122110.
- (22) Zen, A.; Saphiannikova, M.; Neher, D.; Grenzer, J.; Grigorian, S.; Pietsch, U.; Asawapirom, U.; Janietz, S.; Scherf, U.; Lieberwirth, I.; Wegner, G. Effect of Molecular Weight on the Structure and Crystallinity of Poly(3-hexylthiophene). *Macromolecules* **2006**, *39*, 2162–2171.
- (23) Kline, R. J.; McGehee, M. D.; Kadnikova, E. N.; Liu, J.; Frechet, J. M. J.; Toney, M. F. Dependence of Regioregular Poly(3-hexylthiophene) Film Morphology and Field-Effect Mobility on Molecular Weight. *Macromolecules* **2005**, *38*, 3312–3319.
- (24) Tripathi, A. S. M.; Sadakata, S.; Gupta, R. K.; Nagamatsu, S.; Ando, Y.; Pandey, S. S. Implication of Molecular Weight on Optical and Charge Transport Anisotropy in PQT-C12 Films Fabricated by Dynamic FTM. ACS Appl. Mater. Interfaces 2019, 11, 28088–28095.
- (25) Noriega, R.; Rivnay, J.; Vandewal, K.; Koch, F. P. V.; Stingelin, N.; Smith, P.; Toney, M. F.; Salleo, A. A general relationship between disorder, aggregation and charge transport in conjugated polymers. *Nat. Mater.* **2013**, *12*, 1038–1044.
- (26) Koch, F. P. V.; Rivnay, J.; Foster, S.; Müller, C.; Downing, J. M.; Buchaca-Domingo, E.; Westacott, P.; Yu, L.; Yuan, M.; Baklar, M.; Fei, Z.; Luscombe, C.; McLachlan, M. A.; Heeney, M.; Rumbles, G.; Silva, C.; Salleo, A.; Nelson, J.; Smith, P.; Stingelin, N. The impact of molecular weight on microstructure and charge transport in semicrystalline polymer semiconductors poly(3-hexylthiophene), a model study. *Prog. Polym. Sci.* 2013, 38, 1978–1989.
- (27) Gu, K.; Snyder, C. R.; Onorato, J.; Luscombe, C. K.; Bosse, A. W.; Loo, Y.-L. Assessing the Huang–Brown Description of Tie Chains for Charge Transport in Conjugated Polymers. *ACS Macro Lett.* **2018**, *7*, 1333–1338.
- (28) Nikolka, M.; Hurhangee, M.; Sadhanala, A.; Chen, H.; McCulloch, I.; Sirringhaus, H. Correlation of Disorder and Charge Transport in a Range of Indacenodithiophene-Based Semiconducting Polymers. *Adv. Electron. Mater.* **2018**, *4*, No. 1700410.
- (29) Zhao, B.; Pei, D.; Jiang, Y.; Wang, Z.; An, C.; Deng, Y.; Ma, Z.; Han, Y.; Geng, Y. Simultaneous Enhancement of Stretchability, Strength, and Mobility in Ultrahigh-Molecular-Weight Poly-(indacenodithiophene-co-benzothiadiazole). *Macromolecules* **2021**, *54*, 9896–9905.

- (30) Donley, C. L.; Zaumseil, J.; Andreasen, J. W.; Nielsen, M. M.; Sirringhaus, H.; Friend, R. H.; Kim, J.-S. Effects of Packing Structure on the Optoelectronic and Charge Transport Properties in Poly(9,9-di-n-octylfluorene-alt-benzothiadiazole). *J. Am. Chem. Soc.* **2005**, *127*, 12890–12899.
- (31) Zhao, Z.; Yin, Z.; Chen, H.; Zheng, L.; Zhu, C.; Zhang, L.; Tan, S.; Wang, H.; Guo, Y.; Tang, Q.; Liu, Y. High-Performance, Air-Stable Field-Effect Transistors Based on Heteroatom-Substituted Naphthalenediimide-Benzothiadiazole Copolymers Exhibiting Ultrahigh Electron Mobility up to 8.5 cm²/Vs. Adv. Mater. 2017, 29, No. 1602410.
- (32) Zheng, Y.-Q.; Lei, T.; Dou, J.-H.; Xia, X.; Wang, J.-Y.; Liu, C.-J.; Pei, J. Strong Electron-Deficient Polymers Lead to High Electron Mobility in Air and Their Morphology-Dependent Transport Behaviors. *Adv. Mater.* **2016**, *28*, 7213–7219.
- (33) Wang, Y.; Guo, H.; Harbuzaru, A.; Uddin, M. A.; Arrechea-Marcos, I.; Ling, S.; Yu, J.; Tang, Y.; Sun, H.; López Navarrete, J. T.; Ortiz, R. P.; Woo, H. Y.; Guo, X. (Semi)ladder-Type Bithiophene Imide-Based All-Acceptor Semiconductors: Synthesis, Structure—Property Correlations, and Unipolar n-Type Transistor Performance. *J. Am. Chem. Soc.* **2018**, *140*, 6095—6108.
- (34) Feng, K.; Guo, H.; Sun, H.; Guo, X. n-Type Organic and Polymeric Semiconductors Based on Bithiophene Imide Derivatives. *Acc. Chem. Res.* **2021**, *54*, 3804–3817.
- (35) Jenekhe, S. A.; Lu, L.; Alam, M. M. New Conjugated Polymers with Donor–Acceptor Architectures: Synthesis and Photophysics of Carbazole–Quinoline and Phenothiazine–Quinoline Copolymers and Oligomers Exhibiting Large Intramolecular Charge Transfer. *Macromolecules* **2001**, *34*, 7315–7324.
- (36) Agrawal, A. K.; Jenekhe, S. A. New conjugated polyanthrazolines containing thiophene moieties in the main chain. *Macromolecules* **1991**, *24*, 6806–6808.
- (37) Guo, X.; Watson, M. D. Conjugated Polymers from Naphthalene Bisimide. *Org. Lett.* **2008**, *10*, 5333–5336.
- (38) Zhou, N.; Dudnik, A. S.; Li, T.; Manley, E. F.; Aldrich, T. J.; Guo, P.; Liao, H.-C.; Chen, Z.; Chen, L. X.; Chang, R. P. H.; Facchetti, A.; Olvera de la Cruz, M.; Marks, T. J. All-Polymer Solar Cell Performance Optimized via Systematic Molecular Weight Tuning of Both Donor and Acceptor Polymers. *J. Am. Chem. Soc.* **2016**, *138*, 1240–1251.
- (39) Chen, S.; An, Y.; Dutta, G. K.; Kim, Y.; Zhang, Z.-G.; Li, Y.; Yang, C. A Synergetic Effect of Molecular Weight and Fluorine in All-Polymer Solar Cells with Enhanced Performance. *Adv. Funct. Mater.* **2017**, 27, No. 1603564.
- (40) Kolhe, N. B.; Lee, H.; Kuzuhara, D.; Yoshimoto, N.; Koganezawa, T.; Jenekhe, S. A. All-Polymer Solar Cells with 9.4% Efficiency from Naphthalene Diimide-Biselenophene Copolymer Acceptor. *Chem. Mater.* **2018**, *30*, 6540–6548.
- (41) Tran, D. K.; Robitaille, A.; Hai, I. J.; Ding, X.; Kuzuhara, D.; Koganezawa, T.; Chiu, Y.-C.; Leclerc, M.; Jenekhe, S. A. Elucidating the impact of molecular weight on morphology, charge transport, photophysics and performance of all-polymer solar cells. *J. Mater. Chem. A* **2020**, *8*, 21070–21083.
- (42) Deshmukh, K. D.; Matsidik, R.; Prasad, S. K. K.; Connal, L. A.; Liu, A. C. Y.; Gann, E.; Thomsen, L.; Hodgkiss, J. M.; Sommer, M.; McNeill, C. R. Tuning the Molecular Weight of the Electron Accepting Polymer in All-Polymer Solar Cells: Impact on Morphology and Charge Generation. *Adv. Funct. Mater.* **2018**, 28, No. 1707185.
- (43) Choi, J.; Kim, W.; Kim, D.; Kim, S.; Chae, J.; Choi, S. Q.; Kim, F. S.; Kim, T.-S.; Kim, B. J. Importance of Critical Molecular Weight of Semicrystalline n-Type Polymers for Mechanically Robust, Efficient Electroactive Thin Films. *Chem. Mater.* **2019**, *31*, 3163–3173.
- (44) Karpov, Y.; Zhao, W.; Raguzin, I.; Beryozkina, T.; Bakulev, V.; Al-Hussein, M.; Häußler, L.; Stamm, M.; Voit, B.; Facchetti, A.; Tkachov, R.; Kiriy, A. Influence of Semiconductor Thickness and Molecular Weight on the Charge Transport of a Naphthalenediimide-Based Copolymer in Thin-Film Transistors. ACS Appl. Mater. Interfaces 2015, 7, 12478–12487.

- (45) Nahid, M. M.; Matsidik, R.; Welford, A.; Gann, E.; Thomsen, L.; Sommer, M.; McNeill, C. R. Unconventional Molecular Weight Dependence of Charge Transport in the High Mobility n-type Semiconducting Polymer P(NDI2OD-T2). *Adv. Funct. Mater.* **2017**, 27, No. 1604744.
- (46) Zhao, K.; Zhang, T.; Zhang, L.; Li, J.; Li, H.; Wu, F.; Chen, Y.; Zhang, Q.; Han, Y. Role of Molecular Weight in Microstructural Transition and Its Correlation to the Mechanical and Electrical Properties of P(NDI2OD-T2) Thin Films. *Macromolecules* **2021**, *54*, 10203–10215.
- (47) Ito, Y.; Virkar, A. A.; Mannsfeld, S.; Oh, J. H.; Toney, M.; Locklin, J.; Bao, Z. Crystalline Ultrasmooth Self-Assembled Monolayers of Alkylsilanes for Organic Field-Effect Transistors. *J. Am. Chem. Soc.* **2009**, *131*, 9396–9404.
- (48) Sun, Y.; Seo, J. H.; Takacs, C. J.; Seifter, J.; Heeger, A. J. Inverted Polymer Solar Cells Integrated with a Low-Temperature-Annealed Sol-Gel-Derived ZnO Film as an Electron Transport Layer. *Adv. Mater.* **2011**, 23, 1679–1683.
- (49) Courtright, B. A. E.; Jenekhe, S. A. Polyethylenimine Interfacial Layers in Inverted Organic Photovoltaic Devices: Effects of Ethoxylation and Molecular Weight on Efficiency and Temporal Stability. ACS Appl. Mater. Interfaces 2015, 7, 26167–26175.
- (50) Luzio, A.; Criante, L.; D'Innocenzo, V.; Caironi, M. Control of charge transport in a semiconducting copolymer by solvent-induced long-range order. *Sci. Rep.* **2013**, *3*, No. 3425.
- (51) Hwang, Y.-J.; Murari, N. M.; Jenekhe, S. A. New n-type polymer semiconductors based on naphthalene diimide and selenophene derivatives for organic field-effect transistors. *Polym. Chem.* **2013**, *4*, 3187–3195.
- (52) Wu, H.-Y.; Yang, C.-Y.; Li, Q.; Kolhe, N. B.; Strakosas, X.; Stoeckel, M.-A.; Wu, Z.; Jin, W.; Savvakis, M.; Kroon, R.; Tu, D.; Woo, H. Y.; Berggren, M.; Jenekhe, S. A.; Fabiano, S. Influence of Molecular Weight on the Organic Electrochemical Transistor Performance of Ladder-Type Conjugated Polymers. *Adv. Mater.* 2022, 34, No. 2106235.
- (53) Pei, D.; Wang, Z.; Peng, Z.; Zhang, J.; Deng, Y.; Han, Y.; Ye, L.; Geng, Y. Impact of Molecular Weight on the Mechanical and Electrical Properties of a High-Mobility Diketopyrrolopyrrole-Based Conjugated Polymer. *Macromolecules* **2020**, 53, 4490–4500.
- (54) Su, N.; Ma, R.; Li, G.; Liu, T.; Feng, L.-W.; Lin, C.; Chen, J.; Song, J.; Xiao, Y.; Qu, J.; Lu, X.; Sangwan, V. K.; Hersam, M. C.; Yan, H.; Facchetti, A.; Marks, T. J. High-Efficiency All-Polymer Solar Cells with Poly-Small-Molecule Acceptors Having π-Extended Units with Broad Near-IR Absorption. ACS Energy Lett. 2021, 6, 728–738.
- (55) Rivnay, J.; Noriega, R.; Kline, R. J.; Salleo, A.; Toney, M. F. Quantitative analysis of lattice disorder and crystallite size in organic semiconductor thin films. *Phys. Rev. B* **2011**, *84*, No. 045203.
- (56) Rivnay, J.; Mannsfeld, S. C. B.; Miller, C. E.; Salleo, A.; Toney, M. F. Quantitative Determination of Organic Semiconductor Microstructure from the Molecular to Device Scale. *Chem. Rev.* **2012**, *112*, 5488–5519.
- (57) Tsao, H. N.; Cho, D. M.; Park, I.; Hansen, M. R.; Mavrinskiy, A.; Yoon, D. Y.; Graf, R.; Pisula, W.; Spiess, H. W.; Müllen, K. Ultrahigh Mobility in Polymer Field-Effect Transistors by Design. *J. Am. Chem. Soc.* **2011**, *133*, 2605–2612.
- (58) Coropceanu, V.; Cornil, J.; da Silva Filho, D. A.; Olivier, Y.; Silbey, R.; Brédas, J.-L. Charge Transport in Organic Semiconductors. *Chem. Rev.* **2007**, *107*, 926–952.
- (59) Gu, K.; Loo, Y.-L. The Polymer Physics of Multiscale Charge Transport in Conjugated Systems. *J. Polym. Sci., Part B: Polym. Phys.* **2019**, *57*, 1559–1571.
- (60) Noriega, R. Efficient Charge Transport in Disordered Conjugated Polymer Microstructures. *Macromol. Rapid Commun.* **2018**, 39, No. 1800096.
- (61) Babel, A.; Jenekhe, S. A. Morphology and Field-Effect Mobility of Charge Carriers in Binary Blends of Poly(3-hexylthiophene) with Poly[2-methoxy-5-(2-ethylhexoxy)-1,4-phenylenevinylene] and Polystyrene. *Macromolecules* **2004**, *37*, 9835–9840.

(62) McCulloch, I.; Heeney, M.; Chabinyc, M. L.; DeLongchamp, D.; Kline, R. J.; Colle, M.; Duffy, W.; Fischer, D.; Gundlach, D.; Hamadani, B.; Hamilton, R.; Richter, L.; Salleo, A.; Shkunov, M.; Sparrowe, D.; Tierney, S.; Zhang, W. Semiconducting Thienothiophene Copolymers: Design, Synthesis, Morphology, and Performance in Thin-Film Organic Transistors. *Adv. Mater.* 2009, 21, 1091–1109.

□ Recommended by ACS

Enhancing the Backbone Coplanarity of n-Type Copolymers for Higher Electron Mobility and Stability in Organic Electrochemical Transistors

Iuliana P. Maria, Iain McCulloch, et al.

SEPTEMBER 27, 2022 CHEMISTRY OF MATERIALS

READ 🗹

Addition of Low-Molecular-Weight Batches Enhances Charge-Transport Properties of n-Type Polymer Semiconductors

Donguk Kim, Felix Sunjoo Kim, et al.

OCTOBER 05, 2022 MACROMOLECULES

READ **'**

Revealing the "AABB/ABAB Sequential Isomeric Effect" on Diketopyrrole-Based All-acceptor Semiconducting Polymers

Feng Ye, Yuguang Ma, et al.

OCTOBER 06, 2022

ACS APPLIED POLYMER MATERIALS

READ 🗹

Isomeric Acceptor–Acceptor Polymers: Enabling Electron Transport with Strikingly Different Semiconducting Properties in *n*-Channel Organic Thin-Film Transistors

Yongqiang Shi, Yunqi Liu, et al. JANUARY 26, 2022

CHEMISTRY OF MATERIALS

READ 🗹

Get More Suggestions >